

Interact2Ar: Full-Body Human-Human Interaction Generation via Autoregressive Diffusion Models

Pablo Ruiz-Ponce^{1,2}, Sergio Escalera³, José García-Rodríguez²,
Jiankang Deng⁴, Rolandos Alexandros Potamias^{1,4}

¹Huawei Noah's Ark Lab, ²Universidad de Alicante,
³Universitat de Barcelona and Computer Vision Center, ⁴Imperial College London
<https://pabloruizponce.com/papers/Interact2Ar>

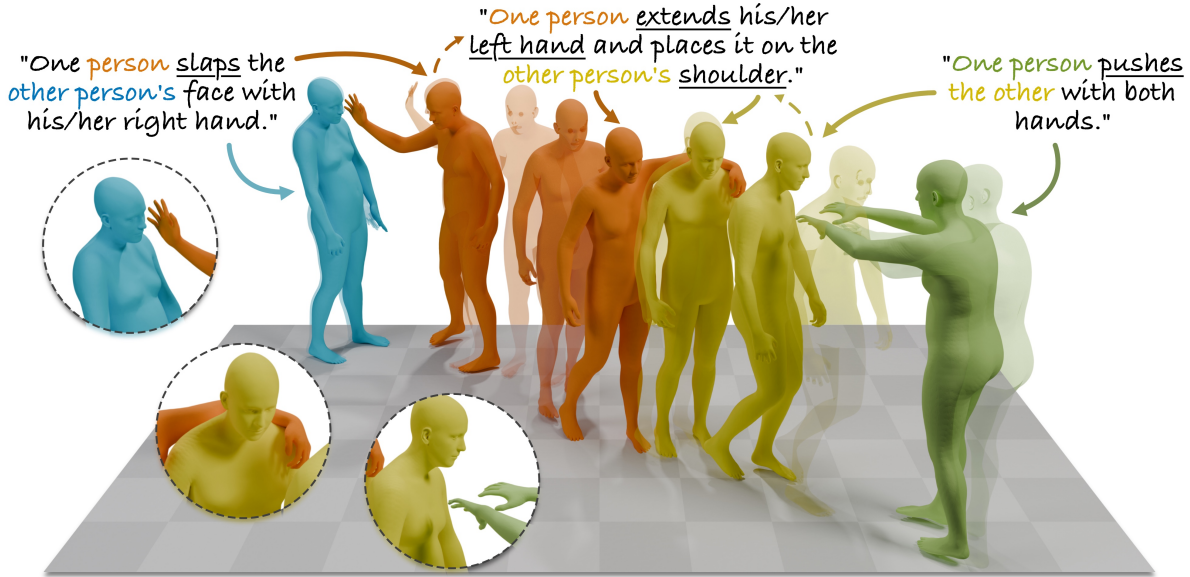


Figure 1. We introduce **Interact2Ar**, the first text-conditioned autoregressive diffusion model for generating full-body human-human interactions with detailed hand motions. Our autoregressive model, with a novel memory strategy, enhances the quality of the generated interaction and enables adaptive capabilities, including temporal composition, adaptation to disturbances, and multi-person scenarios.

Abstract

Generating realistic human-human interactions is a challenging task that requires not only high-quality individual body and hand motions, but also coherent coordination among all interactants. Due to limitations in available data and increased learning complexity, previous methods tend to ignore hand motions, limiting the realism and expressivity of the interactions. Additionally, current diffusion-based approaches generate entire motion sequences simultaneously, limiting their ability to capture the reactive and adaptive nature of human interactions. To address these limitations, we introduce *Interact2Ar*, the first end-to-end text-conditioned autoregressive diffusion model for generating full-body, human-human interactions. *Interact2Ar* incorporates detailed hand kinematics through dedicated parallel branches, enabling high-fidelity full-body generation. Furthermore, we introduce an autoregressive pipeline cou-

pled with a novel memory technique that facilitates adaptation to the inherent variability of human interactions using efficient large context windows. The adaptability of our model enables a series of downstream applications, including temporal motion composition, real-time adaptation to disturbances, and extension beyond dyadic to multi-person scenarios. To validate the generated motions, we introduce a set of robust evaluators and extended metrics designed specifically for assessing full-body interactions. Through quantitative and qualitative experiments, we demonstrate the state-of-the-art performance of *Interact2Ar*.

1. Introduction

Synthesizing realistic human-human interactions remains a formidable challenge in motion generation [67]. Success requires a model that not only generates high-quality motions for individuals but also coherently accounts for the positioning and dynamics of all participants in the inter-

action. A primary obstacle limiting the development of such models is the scarcity of high-quality motion capture data [36], a problem more pronounced in this domain than in other generative fields like text and images. Although datasets for single-human motion have driven recent advances [13, 26, 32], data for multi-person interaction have remained limited. Previous interaction datasets exhibited significant limitations, lacking interaction diversity [29, 46], sufficient textual annotations [10, 48, 54], and hand motion data [23]. The recent introduction of the Inter-X dataset [52], which provides full-body interaction data including detailed hand motions, has been instrumental in addressing these limitations and serves as the basis for training our model, Interact2Ar.

Hand motions provide substantial information in human interactions. Hence, hand modeling is an essential part of non-verbal communication and necessary for capturing contacts between humans. Nevertheless, integrating detailed hand kinematics into human motion generation models presents a significant challenge. The dimensionality of the hands alone exceeds that of the rest of the body. This overhead can introduce more noise than signal, complicating the generation process and leading many models to omit hand information [13, 23, 41, 43, 44]. Previous approaches have attempted to incorporate hands by modeling them separately, using parallel [16] or conditional networks [11]. However, these methods suffer from inefficiency or a lack of body context. This problem is compounded in multi-person scenarios where the dimensionality of the interaction scales with the number of individuals. To overcome this, we introduce an end-to-end architecture that leverages cooperative denoisers for effective information flow between individuals. For full-body generation, we employ dedicated branches that generate hands, body, and global trajectory motions in parallel, where each branch is conditioned on a common encoded representation of the motion from the previous denoising step. This unified approach allows for an efficient yet contextually informed generation process, achieving state-of-the-art (SOTA) performance on the Inter-X benchmark.

Despite the architectural advance of specialized heads, current diffusion-based generation pipelines have inherent limitations. These models typically denoise the entire motion sequence at once. While effective for single-human scenarios, this holistic approach struggles to capture the high variability and temporally reactive nature of human interactions, where each person’s motions are contingent on the subtle cues of their interaction partner. We therefore introduce the first, to the best of our knowledge, end-to-end text-conditioned autoregressive diffusion model for generating full-body interactions. By generating the motion sequentially, our model can better adapt to the evolving dynamics of the interaction, further improving upon the results

obtained by our non-autoregressive approach. To increase the efficiency of memory management, we propose a Mixed Memory approach, where short- and long-term information is included at different frame rates. As a result, a series of additional adaptive interactions are enabled by our model, including temporal motion composition, adaptation to random displacements, and extension to multi-human scenarios beyond dyadic interactions.

To evaluate all these contributions, a robust and detailed evaluation pipeline is needed. In addition to general evaluation metrics, we extend previous quantitative evaluation pipelines to include body-part-specific evaluators that provide detailed insights about motion quality. We also increased their robustness by retraining all evaluators with the global positions of the interactants instead of rotation-based representations. Finally, we included jerk-based metrics to evaluate the smoothness of transitions, which is particularly important for assessing the new downstream capabilities of our autoregressive model.

The main contributions of this paper are as follows:

- We propose an end-to-end diffusion model for generating human-human interactions with detailed hand motions, achieving state-of-the-art performance on Inter-X.
- We introduce an autoregressive diffusion pipeline for human-human interaction generation that improves interaction quality through sequential motion synthesis with efficient memory management. Its adaptability enables downstream tasks, including temporal composition, disturbance adaptation, and multi-human generation.
- We extend quantitative evaluation by proposing more robust and specialized evaluators, enabling more reliable and informative assessment.

2. Related Work

Human Motion Generation. The field of human motion generation has experienced remarkable growth in recent years [67], driven by the introduction of large-scale datasets [3, 12, 13, 18, 26, 33, 38, 51] and novel generative architectures [12, 15, 43, 44]. However, such rapid expansion has introduced several challenges that distinguish this area from more mature research domains. One issue is the lack of standardized data representations [13, 23, 25, 27, 30, 55]. While certain representations are designed to facilitate the computation of kinematic losses and to improve model learning [13, 23, 55], they suffer from memory inefficiency. Another challenge is the integration of hand kinematics, which are frequently omitted due to their high dimensionality and susceptibility to noise [13, 43, 44], despite their critical role in expressive motion synthesis. Additionally, there is no established generative paradigm that consistently outperforms others. Diffusion-based approaches [1, 7, 17, 22, 44, 57, 59, 60, 65] typically deliver superior motion quality and greater adaptability to diverse

conditions, but at the cost of slower inference and more intensive training requirements. Conversely, quantized representation methods [14, 15, 21, 31, 56, 58, 61, 64] offer faster training and inference, and their learned discrete tokens enable robust motion quality with minimal tuning, though with reduced flexibility in conditioning and control. Finally, evaluation remains a significant challenge. While standard metrics provide a general assessment of model performance, recent studies [27, 28] have exposed their limitations. These studies reveal biases toward certain architectures and question their reliability as indicators of true motion quality.

Human-Human Interaction Generation. Generating human-human interactions substantially amplifies the challenges inherent in single-person motion synthesis [9, 40]. While progress has been facilitated by different datasets [10, 29, 46, 48, 54], with the most recent ones being InterHuman [23] and Inter-X [52], the modeling complexity is considerably higher than for single-human motions. Unlike single-person scenarios, models must learn intricate spatio-temporal dependencies to ensure that each agent’s motion remains coherent with respect to others. Capturing the full distribution of human interactions represents a formidable challenge that current datasets only partially address. Inter-X has enabled new research directions in full-body interaction generation, including detailed hand articulation, which is frequently omitted due to its modeling complexity [23, 35, 41]. Several approaches have tackled interaction modeling through different architectural paradigms [4, 37, 41, 42, 47, 53, 55]. InterGen [23] and in2IN [35] employed diffusion models with cooperative denoising mechanisms to capture inter-agent dependencies. More recently, InterMask [19] introduced residual VQ-VAE masked transformers for interaction generation, achieving state-of-the-art performance on the Inter-X benchmark. Our work proposes a novel diffusion-based model with body-specific heads capable of synthesizing high-fidelity human-human interactions with detailed hand dynamics, achieving state-of-the-art results on the Inter-X benchmark.

Autoregressive Diffusion Models for Human Motion Generation. A key limitation of diffusion models in human motion generation is their tendency to generate entire motion sequences in a single forward pass [44]. While this approach may suffice for simple, isolated single-person scenarios, it fails to capture the dynamic, responsive nature of humans interacting in the real world. Recently, autoregressive diffusion models have been introduced to generate short motion segments conditioned on a temporal context window [6, 39, 49, 63]. This paradigm has enabled single-person motion generation systems to exhibit greater responsiveness to diverse inputs, such as environmental context [45] and external physical forces [62]. More recently, autoregressive diffusion has shown promising re-

sults in reaction generation tasks [5, 20]. To the best of our knowledge, our work presents the first end-to-end text-conditioned autoregressive diffusion model for full-body human-human interactions. The rationale for adopting this paradigm is that autoregressive generation enables dynamic adaptation of each individual’s motion based on their partner’s movements and the evolving interaction context. This approach yields models capable of capturing the inherent variability and responsiveness of human-human interactions. We demonstrate this capability through a series of downstream tasks that evaluate the model’s adaptability to dynamic interaction scenarios.

3. Method

Interact2Ar generates full-body human-human interactions x conditioned on textual descriptions c . We present a diffusion model (Sec. 3.2) using cooperative denoisers to facilitate information flow between interactants, along with specialized branches for generating the different body parts. We further improve our denoiser architecture with an autoregressive pipeline (Sec. 3.3) that replaces full motion generation with a step-wise approach where the denoiser predicts sub-motions while retaining a prefix of predefined length from the previous sub-motions as memory. To improve memory management, we propose a mixed strategy (Sec. 3.3) that efficiently provides both short-term and long-term information. All these methodological contributions provide adaptive capabilities to Interact2Ar that enable additional downstream applications (Sec. 3.4).

3.1. Dataset & Motion Representation

Inter-X [52] is the most suitable dataset for training Interact2Ar as it contains 11K full-body interactions performing 40 different actions with detailed textual descriptions.

Redundant representations, where certain features can be derived from others (e.g., joint velocities from positions), have become common in human motion modeling, as they facilitate learning and accelerate the computation of certain losses during training. However, this approach increases feature dimensionality, which becomes especially problematic when representing two individuals with detailed hand articulations. Furthermore, redundant representations are suboptimal for diffusion model evaluation pipelines, as they introduce negative biases [28]. To address these issues, we rely exclusively on SMPL-X parameters [30] to represent interactions. A dyadic interaction $x = \{^a x, ^b x\}$ between individuals a and b is composed of individual poses, where each $^i x$ is represented as $(r, \varphi, \theta_{\text{body}}, \theta_{\text{hands}})$, with $r \in \mathbb{R}^3$ denoting the root translation, and $\varphi \in \mathbb{R}^6, \theta_{\text{body}} \in \mathbb{R}^{21 \times 6}, \theta_{\text{hands}} \in \mathbb{R}^{30 \times 6}$ representing the root and joint rotations using the continuous 6D representation [66]. Since the dataset exhibits limited body shape diversity, we normalize all shapes to a neutral body configuration.

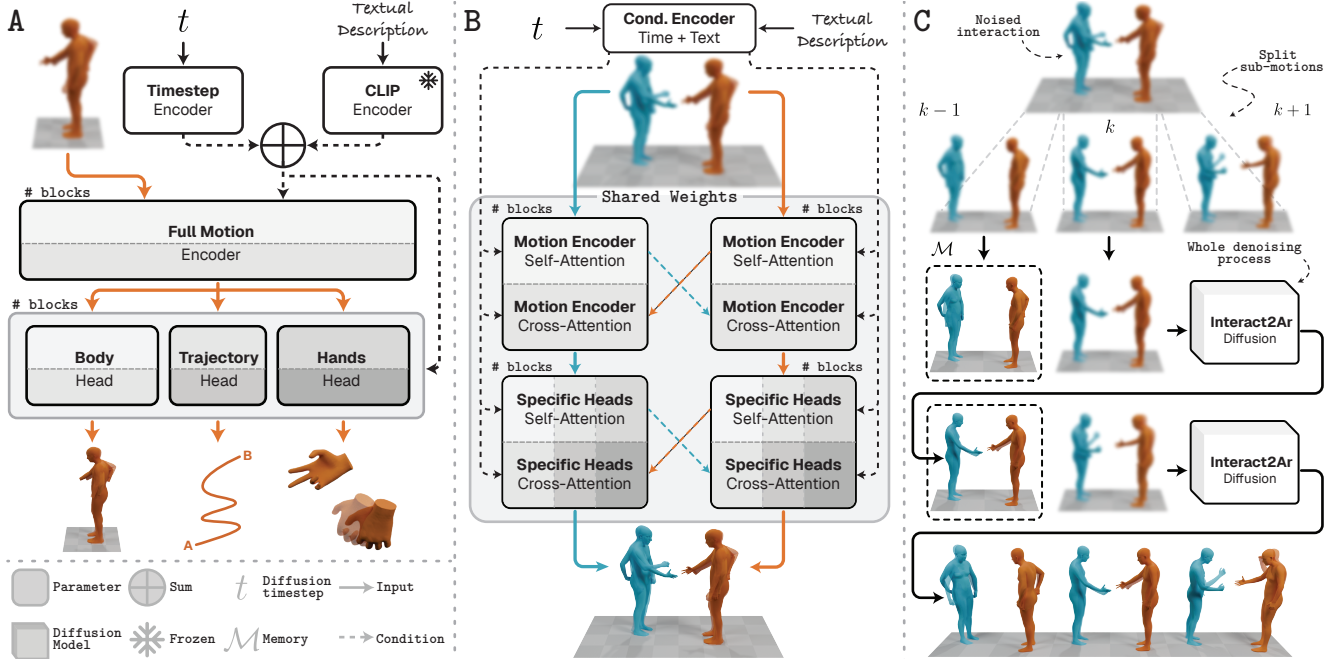


Figure 2. **A) Multi-Head Denoiser:** An encoder feeds noised motion and condition information to specialized heads for body, trajectory, and hands denoising. **B) Cooperative Denoisers:** Parallel streams with shared weights generate each interactant while cross-attention shares inter-personal information. **C) Autoregressive:** Sequential generation of sub-motions conditioned on previously generated frames.

3.2. Full-Body Interaction Generation

For generating human-human interactions, we employ diffusion models for their quality and adaptability [8, 36, 50]. In this paradigm, we incrementally add Gaussian noise $\mathcal{N}(0, 1)$ to the motions and train a denoising network that learns to incrementally remove the added noise. The denoiser takes as input the textual condition c and the partially noised interaction x^t , and predicts \hat{x}^{t-1} , where t represents the step in the diffusion chain and the hat notation denotes a prediction made by our model. We follow [34, 44] and directly predict \hat{x}^0 at each denoising step, instead of \hat{x}^{t-1} , to enable the calculation of kinematic losses.

Architecture. We build upon the cooperative denoiser architecture proposed by InterGen [23]. This transformer-encoder architecture processes each individual in parallel through separate streams that share weights. To flow information between individuals, hidden states are exchanged between streams via cross-attention. This design choice enables a more compact network with fewer trainable parameters while preserving interaction information.

However, this architecture predicts entire pose sequences without body-part specialization, which can hinder accurate modeling of high-dimensional representations, particularly for complex hand articulations. We address this by introducing an initial encoding module that maps noised motion into a latent representation, which feeds three specialized denoising heads for global trajectory, body poses, and hand poses. This design enables body-specific modules that

leverage full motion information for coherent predictions while allowing parallel computation across heads. The architecture is illustrated in Fig. 2.

Training Losses. We adopt a combination of commonly used losses for training diffusion models in the task of human-human interaction generation [23, 35]:

$$\begin{aligned} \mathcal{L}_{\text{total}} = & \lambda_{\text{repr}} \mathcal{L}_{\text{repr}}(x, \hat{x}) + \lambda_{\text{orient}} \mathcal{L}_{\text{orient}}(r, \hat{r}) \\ & + \lambda_{\text{pos}} \mathcal{L}_{\text{pos}}(p, \hat{p}) + \lambda_{\text{vel}} \mathcal{L}_{\text{vel}}(v, \hat{v}) \\ & + \lambda_{\text{foot}} \mathcal{L}_{\text{foot}}(f, \hat{f}) + \lambda_{\text{dist}} \mathcal{L}_{\text{dist}}(d, \hat{d}), \end{aligned} \quad (1)$$

where $\mathcal{L}_{\text{repr}}$ is the ℓ_2 loss between raw SMPL-X representations, $\mathcal{L}_{\text{orient}}$ penalizes root orientation errors, and the remaining four terms are kinematic losses computed via forward kinematics (FK). To compute these, we pass predicted SMPL-X parameters through a differentiable FK layer to obtain joint positions $p = \text{FK}(x)$ and $\hat{p} = \text{FK}(\hat{x})$, from which we compute: \mathcal{L}_{pos} for global joint positions, \mathcal{L}_{vel} for joint velocities, $\mathcal{L}_{\text{foot}}$ for foot contacts, and $\mathcal{L}_{\text{dist}}$ for pairwise joint distance maps between individuals. Weighting coefficients $\{\lambda_i\}$ were tuned through grid search. Additional details are provided in the Supplementary Material.

3.3. Autoregressive Interaction Generation

Unlike single-human motion generation, human-human interaction requires a high level of adaptability to respond to changes in the interaction state. Traditional diffusion methods employed for motion generation cannot achieve this

level of adaptability as they predict the entire sequence at once. We extend our denoiser by proposing an autoregressive diffusion pipeline for human-human interaction following the advancements in single-human scenarios [45].

An interaction x of total length N is decomposed into a series of contiguous non-overlapping sub-motions:

$$x = \bigcup_{k=0}^{K-1} x_{kn:(k+1)n}, \quad (2)$$

where $K = \lceil N/n \rceil$ denotes the number of sub-motions, and n represents the generation window, i.e., the number of frames the denoiser can output in a single forward pass. At each generation step k , the denoiser predicts the next sub-motion conditioned on a short-term memory buffer \mathcal{M}^s of the m_s most recent previously generated frames:

$$\mathcal{M}_k^s = x_{kn-m_s:kn}^0 \quad (3)$$

The denoiser then predicts:

$$\hat{x}_{kn:(k+1)n}^0 = G(x_{kn:(k+1)n}^t, \mathcal{M}_k^s, c, t), \quad (4)$$

where $x_{kn:(k+1)n}^t$ is the noised sub-motion at diffusion timestep t , c is the textual condition, and t is the current diffusion timestep. The memory size m_s controls the temporal context available to the model, allowing it to maintain coherence with past motions while generating new frames.

Mixed Memory. A key limitation of this approach is the constrained short-term memory capacity. Recent works typically employ prediction windows of 20 to 40 frames, with memory windows of a similar range [45, 62]. While this can be sufficient for short or repetitive motions, our observations indicate that for long-duration interactions (Fig. 3), such limited memory adversely affects output quality, resulting in repetitive motion artifacts due to insufficient historical context.

To address this limitation, we augment the short-term memory with a long-term component \mathcal{M}^l . We maintain a temporally downsampled history spanning a substantially longer window by retaining frames at intervals of δ over a temporal window of m_l frames, where $m_l \gg m_s$:

$$\mathcal{M}_k^l = \{x_{kn-m_l+i\delta}^0 \mid i = 0, 1, \dots, \lfloor m_l/\delta \rfloor\} \quad (5)$$

The complete memory buffer is constructed by concatenating both components:

$$\mathcal{M}_k = \{\mathcal{M}_k^l, \mathcal{M}_k^s\} \quad (6)$$

The denoiser now predicts conditioned on Mixed Memory:

$$\hat{x}_{kn:(k+1)n}^0 = G(x_{kn:(k+1)n}^t, \mathcal{M}_k, c, t) \quad (7)$$

Our dual-memory architecture enables the model to leverage full-framerate immediate context for seamless transitions and long-range temporal information at a downsampled framerate more efficiently than covering the whole

context window with simple memory. The downsampling rate δ and long-term window size m_l are hyperparameters that control the trade-off between memory coverage and computational efficiency. A graphical illustration of this process is shown in Fig. 3.

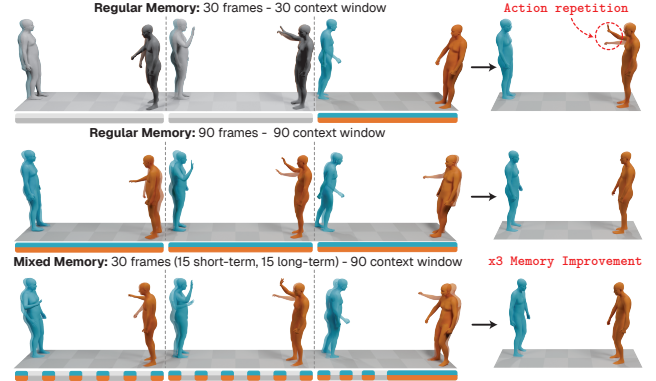


Figure 3. **Mixed Memory** enables access to both detailed short-term information, facilitating seamless transitions, along with long-term context, avoiding action repetition in long interactions. Our proposed Mixed Memory overcomes the limitations of regular context memory, providing up to a $\times 3$ reduction in memory size.

3.4. Adaptive Interactions

Thanks to our proposed autoregressive pipeline with a Mixed Memory strategy, Interact2Ar presents a series of adaptability capabilities that enable several downstream interaction applications. A quantitative and qualitative analysis of these capabilities can be found in Sec. 4.3, and a comparison with previous methods in the Supplementary Video.

Temporal Motion Composition. The autoregressive generation naturally enables temporal composition of different actions with seamless transitions when switching between textual prompts. Because the denoiser conditions on the memory buffer \mathcal{M} from previously generated sub-motions, it natively handles compositional transitions during generation without requiring offline post-processing or suffering from the global positioning misalignments common in inpainting-based approaches.

Real-Time Disturbance Adaptation. The step-wise generation paradigm enables real-time adaptation to external disturbances. By generating sub-motions of length n conditioned on recent history, the model can adapt to significant state perturbations between generation steps (e.g., sudden position changes, unexpected contact events), demonstrating reactive generation beyond pre-planned sequences.

Sequential Multi-Person Interactions. Combining temporal composition with disturbance adaptation enables scenarios where one individual sequentially interacts with multiple partners. After completing an interaction with one partner, a new interactant can be introduced with a different prompt, and the memory-conditioned generation ensures

smooth transitions between sequential dyadic interactions without requiring simultaneous multi-person modeling.

4. Experimentation

Implementation details. The cooperative denoiser uses 8 transformer blocks with 8 attention heads (latent dimension 512, feed-forward dimension 1024) for the motion encoder and both body and hand pose heads, while the trajectory head uses 4 blocks with 4 heads (latent dimension 256, feed-forward dimension 512). For diffusion steps, the full model uses 1000 steps with DDIM-50 sampling, while the autoregressive version achieves the best empirical results with only 10 steps. All models were trained for 5000 epochs using EMA and AdamW (learning rate 1×10^{-4} , weight decay 2×10^{-5} , batch size 128). Additional implementation details are provided in the Supplementary materials.

Evaluation Metrics. We adopt the widely used metrics [13] for measuring generation quality and textual alignment: R-Precision (R-Prec.), Frechet Inception Distance (FID), MultiModal Distance (MM Dist), Diversity, and MultiModality (MModality). To quantitatively evaluate the adaptive nature of our model, we employ the Peak Jerk (PJ) and Area Under the Jerk (AUJ) metrics from [2] to assess the smoothness transitioning from different states. We generate 64 sequences of 8 temporally concatenated motions each and calculate the PJ and AUJ across the complete sequences, implementing concatenation through inpainting for models lacking native support.

Full Body Evaluation. As we experimentally show in Tab. 1, the original evaluator from Inter-X has serious limitations in recognizing degradation in the interactions. It maintains the same performance even when serious degradation is applied to the trajectory or when the trajectories of the individuals are swapped. To address this, we re-trained the original evaluator using only joint positions instead of rotations to minimize bias and improve evaluation quality [28]. Given the importance of the global position of an individual with respect to another, we opt to use global joint coordinates instead of relative. To enhance the interpretability of full-body evaluation, we train three distinct evaluators for different body components: one for all joints (as in the original benchmark), one for body joints only, and one for hand joints only. In Tab. 1, we can observe that our new evaluators recognize and penalize much more serious degradations than previous evaluators.

4.1. Comparison to State-of-the-art Approaches

Quantitative Evaluation. Tab. 2 presents the quantitative comparison of Interact2Ar against previous state-of-the-art (SOTA) methods across different aspects and levels of detail. In terms of motion quality, both the non-autoregressive and autoregressive versions of Interact2Ar surpass the previous SOTA, InterMask. Examining the

results more closely reveals improvements in the evaluation metrics for body and hands independently. These results demonstrate that our proposed cooperative denoiser architecture handles this full-body motion representation substantially better than previous approaches. Furthermore, the autoregressive version consistently outperforms the non-autoregressive version across all metrics, highlighting the advantages of this paradigm for modeling interactions. Please note that MultiModality metric tends to yield lower values for models that perform better and align more closely to the textual description provided [35].

Method	Prev. Evaluator [52]		Ours	
	R-Prec. \uparrow	FID \downarrow	R-Prec. \uparrow	FID \downarrow
<i>Ground Truth</i>	0.739 \pm .00	0.001 \pm .00	0.740 \pm .00	0.002 \pm .00
Interact2Ar	0.737 \pm .00	0.148 \pm .01	0.773 \pm .00	0.277 \pm .01
+10% noise	0.307 \pm .00	38.35 \pm .12	0.211 \pm .00	74.58 \pm .14
+10% noise traj.	0.737 \pm .00	0.122 \pm .00	0.249 \pm .00	62.05 \pm .12
+ traj. swap	0.729 \pm .00	0.165 \pm .01	0.558 \pm .00	8.65 \pm .05

Table 1. **Evaluator robustness comparison.** Our evaluator demonstrates superior sensitivity to motion quality degradations compared to the previous one. Tested degradations: noise on full representation, noise on trajectory only, and trajectory swapping.

Qualitative Evaluation. Beyond quantitative evaluation, qualitative comparisons better illustrate the differences in quality between previous methods and ours. Our method clearly generates higher-quality interactions with improved alignment to textual descriptions and more realistic hand motions (Fig. 5). The Supplementary Video provides additional qualitative comparisons, allowing for a more comprehensive appreciation of the temporal and spatial coherence and overall realism achieved by our method.

User Study. To assess generation quality, we conducted a user study with 35 participants. Users ranked 10 videos, each containing one interaction extracted from: ground truth, our model, InterMask, and InterGen. For each video, participants ranked the generations based on (1) overall quality and alignment with the textual description, and (2) realism of hand motions. As shown in Fig. 4, our method clearly outperforms previous approaches across both criteria and approaches ground-truth quality.

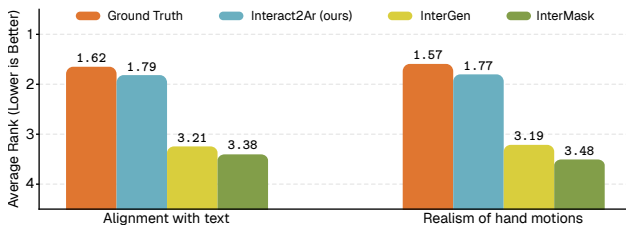


Figure 4. **User study** with the average ranking of 35 participants evaluating the text alignment and hand quality of 10 interactions.

	Methods	R-Precision \uparrow			FID \downarrow	MM Dist \downarrow	Diversity \rightarrow	MModality \uparrow	PJ \uparrow	AUJ \downarrow
		Top 1	Top 2	Top 3						
Full	<i>Ground Truth</i>	0.431 \pm .00	0.631 \pm .00	0.740 \pm .00	0.002 \pm .00	3.318 \pm .01	8.973 \pm .10	-	0.021 \pm .00	3.944 \pm .00
	T2M [13]	0.211 \pm .00	0.339 \pm .00	0.434 \pm .00	9.079 \pm .11	5.766 \pm .02	7.994 \pm .08	0.789 \pm .03	1.889 \pm .12	124.9 \pm 1.9
	InterGen [23]	0.411 \pm .01	0.608 \pm .00	0.721 \pm .00	0.874 \pm .02	3.618 \pm .01	8.876 \pm .07	3.345\pm.07	2.132 \pm .12	84.16 \pm 3.1
	InterMask [19]	0.415 \pm .00	0.607 \pm .00	0.722 \pm .00	0.671 \pm .02	3.487 \pm .01	8.654 \pm .06	1.686 \pm .06	2.328 \pm .21	61.74 \pm .50
	Interact2Ar*	0.436 \pm .00	0.643 \pm .00	0.757 \pm .00	0.556 \pm .02	3.246 \pm .01	8.916\pm.07	2.743 \pm .05	2.110 \pm .17	54.97 \pm .67
	Interact2Ar	0.453\pm.00	0.661\pm.00	0.773\pm.00	0.277\pm.01	3.095\pm.01	9.305 \pm .07	1.427 \pm .04	0.136\pm.00	8.837\pm.17
Body	<i>Ground Truth</i>	0.462 \pm .01	0.655 \pm .00	0.758 \pm .00	0.001 \pm .00	3.272 \pm .01	9.002 \pm .07	-	0.014 \pm .00	3.832 \pm .00
	T2M [13]	0.222 \pm .00	0.354 \pm .00	0.452 \pm .00	3.416 \pm .07	5.436 \pm .02	8.018 \pm .07	0.905 \pm .03	1.857 \pm .10	115.6 \pm 1.7
	InterGen [23]	0.393 \pm .00	0.571 \pm .00	0.671 \pm .00	5.762 \pm .30	4.564 \pm .03	10.45 \pm .09	4.566\pm.13	2.116 \pm .13	77.09 \pm 3.9
	InterMask [19]	0.386 \pm .00	0.565 \pm .01	0.664 \pm .00	6.720 \pm .28	4.616 \pm .03	10.61 \pm .11	2.493 \pm .12	2.549 \pm .16	59.41 \pm .69
	Interact2Ar*	0.426 \pm .00	0.611 \pm .00	0.710 \pm .00	5.728 \pm .29	4.190 \pm .02	10.67 \pm .10	3.967 \pm .13	2.040 \pm .17	53.30 \pm .51
	Interact2Ar	0.469\pm.00	0.672\pm.00	0.779\pm.00	0.352\pm.01	3.173\pm.01	9.271\pm.08	1.421 \pm .04	0.123\pm.00	6.620\pm.13
Hands	<i>Ground Truth</i>	0.399 \pm .00	0.597 \pm .00	0.713 \pm .00	0.002 \pm .00	3.312 \pm .01	8.370 \pm .05	-	0.017 \pm .00	2.480 \pm .00
	T2M [13]	0.196 \pm .00	0.317 \pm .00	0.405 \pm .01	9.424 \pm .12	5.398 \pm .02	6.996 \pm .11	0.791 \pm .04	1.767 \pm .09	113.1 \pm 1.9
	InterGen [23]	0.357 \pm .00	0.536 \pm .01	0.645 \pm .00	1.389 \pm .03	3.806 \pm .02	8.006 \pm .07	3.736\pm.11	2.049 \pm .12	70.47 \pm 2.9
	InterMask [19]	0.360 \pm .00	0.538 \pm .00	0.647 \pm .00	1.960 \pm .05	3.794 \pm .02	7.939 \pm .07	1.895 \pm .09	2.201 \pm .16	59.77 \pm .76
	Interact2Ar*	0.382 \pm .00	0.566 \pm .00	0.678 \pm .00	0.906 \pm .02	3.563 \pm .01	8.273\pm.10	3.206 \pm .09	1.923 \pm .09	51.03 \pm .49
	Interact2Ar	0.422\pm.00	0.629\pm.00	0.745\pm.00	0.257\pm.01	3.111\pm.01	8.614 \pm .08	1.439 \pm .05	0.120\pm.00	7.474\pm.16

Table 2. Comparison of our model (Interact2Ar) to the state of the art in human-human interaction motion generation on the Inter-X dataset. *Interact2Ar model is the version without autoregressive generation. All evaluations have been executed 20 times to elude the randomness of the generation. \pm indicates the 95% confidence interval. We highlight the **best** and the **second best** results.

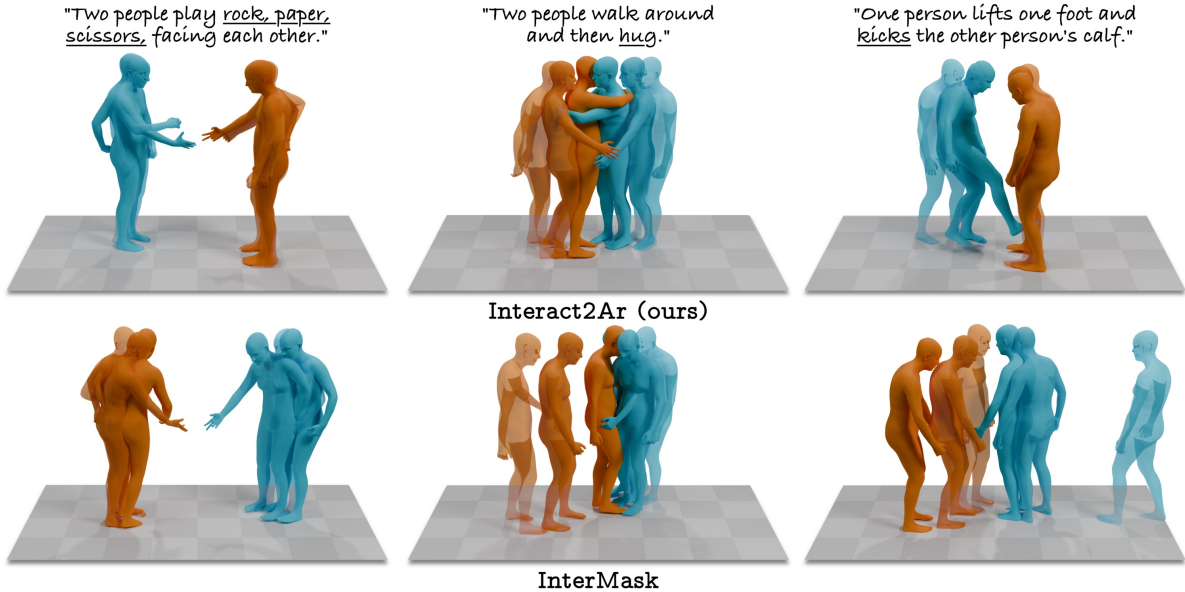


Figure 5. **Interact2Ar comparison with SOTA.** Our method Interact2Ar (top) generates higher-quality interactions with improved alignment to textual descriptions and more realistic hand motions in comparison to the previous SOTA InterMask (bottom).

4.2. Ablation Study

Tab. 3 shows an ablation study of different autoregressive configurations in terms of memory size. We observe that models without Mixed Memory degrade in performance as more memory is added, while those with Mixed Memory maintain better performance with larger contexts. The increase in context, while adding more information to the model, also increases the complexity that the model must

learn. Based on benefits obtained in LLMs from larger contexts [24], having a method that enables large context windows without significant memory overhead is promising. Based on the overall metrics, memory utilization, and qualitative examples, we selected the hyperparameters $m_s = 15$, $m_l = 45$, and $\delta = 5$, which provide a 60-frame context window while using only 24 frames. Additional metrics and experiments are available in the Supplementary Materials.

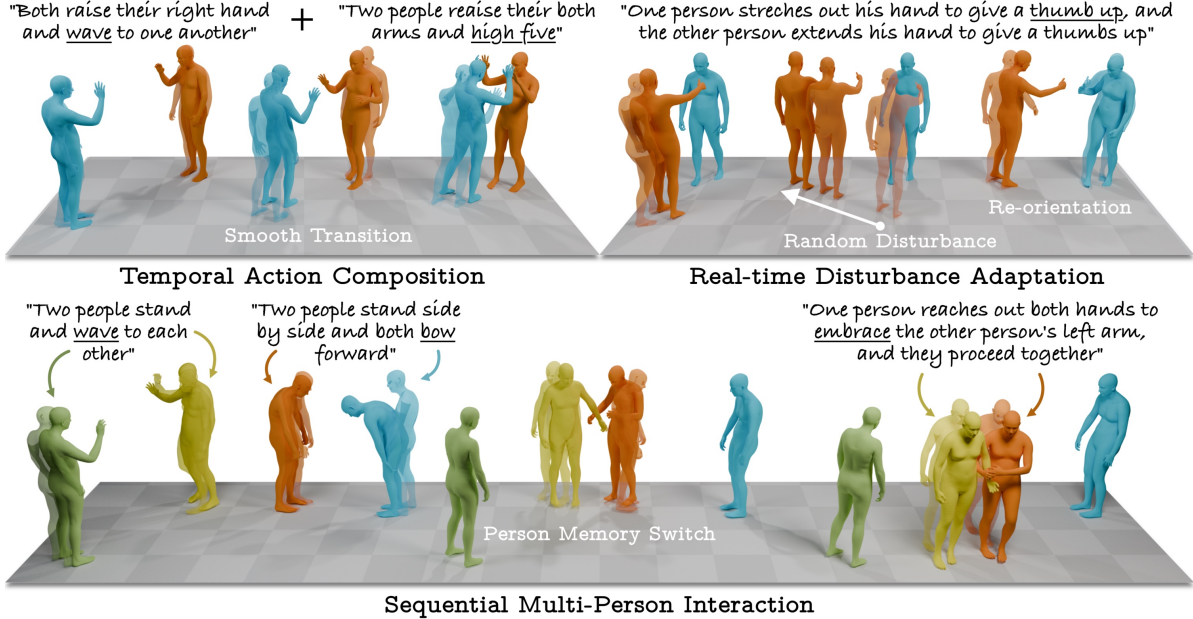


Figure 6. **Interact2Ar Adaptive Interactions.** Our method with autoregressive diffusion and a Mixed Memory strategy enables a series of adaptive downstream tasks, including temporal motion composition, displacement adaptation, and sequential multi-human interactions.

m_s	m_l	\mathcal{M}	R-Prec. \uparrow	FID \downarrow	MM Dist. \downarrow	Div. \rightarrow	MMod. \uparrow
-	-	-	.722 \pm .00	.001 \pm .00	3.34 \pm .00	9.08 \pm .00	-
15	-	15	.765 \pm .00	.283 \pm .00	3.14 \pm .01	9.28 \pm .08	1.49 \pm .05
30	-	30	.769 \pm .00	.346 \pm .01	3.12 \pm .01	9.24 \pm .06	1.47 \pm .04
60	-	60	.776 \pm .00	.316 \pm .01	3.07 \pm .02	9.29 \pm .07	1.39 \pm .06
90	-	90	.771 \pm .00	.412 \pm .01	3.10 \pm .01	9.26 \pm .07	1.34 \pm .04
120	-	120	.774 \pm .00	.413 \pm .01	3.08 \pm .01	9.30 \pm .07	1.34 \pm .04
15	15	18	.769 \pm .00	.289 \pm .01	3.13 \pm .01	9.26 \pm .06	1.46 \pm .05
15	45	24	.773 \pm .00	.277 \pm .01	3.10 \pm .01	9.31 \pm .07	1.43 \pm .04
15	75	30	.771 \pm .00	.279 \pm .01	3.11 \pm .01	9.32 \pm .06	1.35 \pm .05
15	105	36	.773 \pm .00	.325 \pm .01	3.09 \pm .01	9.35 \pm .06	1.36 \pm .04

Table 3. **Ablation study** on memory configurations for Interact2Ar. m_s and m_l represent the context window used for each memory. $m_l = -$ indicates models not using Mixed Memory. For models using Mixed Memory, $\delta = 5$. The total number of frames used in the full memory is $m = m_s + m_l / \delta$.

4.3. Adaptive Interactions

As described in Sec. 3.4, Interact2Ar can seamlessly generate adaptive interactions thanks to our autoregressive diffusion model with Mixed Memory. We quantitatively evaluate this adaptability in terms of transition smoothness using the PJ and AUJ metrics as described at the beginning of this section. Tab. 2 shows that the autoregressive version of Interact2Ar clearly outperforms all previous methods.

Fig. 6 shows our method seamlessly generating smooth temporal motion composition, adapting to random displacements, and handling sequential multi-human interactions. In the Supplementary video, these capabilities are more visually apparent, and comparisons with previous methods show that previous approaches produce highly abrupt transitions as a consequence of overfitting to initial positions.

5. Conclusion

We introduced Interact2Ar, the first text-conditioned autoregressive diffusion model for generating full-body human-human interactions. Our cooperative denoiser architecture, with body-part specialized heads, achieves state-of-the-art performance on the Inter-X benchmark for full-body interaction generation, including detailed hand motions. We validated the quality of generated motions through quantitative and qualitative experiments, proposing a robust set of evaluators that better detect motion degradation and body-part-specific metrics that enable more informative assessment of interaction quality. Building on this foundation, we introduced an autoregressive diffusion pipeline that produces more aligned and adaptable interaction models, improving dyadic interaction generation while enabling downstream applications including temporal motion composition, disturbance adaptation, and multi-human interactions. Finally, our Mixed Memory paradigm leverages short- and long-term information to generate motions with broader temporal context while optimizing memory efficiency.

Limitations and Future Work. Interact2Ar introduces several contributions in full-body human-human interaction generation. However, some limitations originating from dataset constraints shape future work. Accounting for human diversity in realistic interactions requires modeling distinct body shapes. While Inter-X has largely improved over previous datasets in terms of full-body motions, shape distributions remain a challenge. Consequently, the dataset provides body shapes normalized to neutral, which hinders the precision of hand contacts between individuals.

Acknowledgments. This work has been partially supported by the Spanish national grant for PhD studies, FPU22/04200. Additionally, we thank Julian Tanke for fruitful discussions regarding the limitations of current evaluators of human motion models.

References

- [1] Samaneh Azadi, Akbar Shah, Thomas Hayes, Devi Parikh, and Sonal Gupta. Make-an-animation: Large-scale text-conditional 3d human motion generation. In *Proceedings of the IEEE/CVF International Conference on Computer Vision*, pages 15039–15048, 2023. 2
- [2] German Barquero, Sergio Escalera, and Cristina Palmero. Seamless human motion composition with blended positional encodings. In *Proceedings of the IEEE/CVF Conference on Computer Vision and Pattern Recognition*, pages 457–469, 2024. 6
- [3] Zhongang Cai, Daxuan Ren, Ailing Zeng, Zhengyu Lin, Tao Yu, Wenjia Wang, Xiangyu Fan, Yang Gao, Yifan Yu, Liang Pan, Fangzhou Hong, Mingyuan Zhang, Chen Change Loy, Lei Yang, and Ziwei Liu. HuMMan: Multi-modal 4d human dataset for versatile sensing and modeling. In *17th European Conference on Computer Vision, Tel Aviv, Israel, October 23–27, 2022, Proceedings, Part VII*, pages 557–577. Springer, 2022. 2
- [4] Zhongang Cai, Jianping Jiang, Zhongfei Qing, Xinying Guo, Mingyuan Zhang, Zhengyu Lin, Haiyi Mei, Chen Wei, Ruisi Wang, Wanqi Yin, et al. Digital life project: Autonomous 3d characters with social intelligence. In *Proceedings of the IEEE/CVF conference on computer vision and pattern recognition*, pages 582–592, 2024. 3
- [5] Zhi Cen, Huaijin Pi, Sida Peng, Qing Shuai, Yujun Shen, Hujun Bao, Xiaowei Zhou, and Ruizhen Hu. Ready-to-react: Online reaction policy for two-character interaction generation. In *ICLR*, 2025. 3
- [6] Rui Chen, Mingyi Shi, Shaoli Huang, Ping Tan, Taku Komura, and Xuelin Chen. Taming diffusion probabilistic models for character control. In *ACM SIGGRAPH 2024 Conference Papers*, New York, NY, USA, 2024. Association for Computing Machinery. 3
- [7] Xin Chen, Biao Jiang, Wen Liu, Zilong Huang, Bin Fu, Tao Chen, and Gang Yu. Executing your commands via motion diffusion in latent space. In *Proceedings of the IEEE/CVF conference on computer vision and pattern recognition*, pages 18000–18010, 2023. 2
- [8] Prafulla Dhariwal and Alexander Nichol. Diffusion models beat gans on image synthesis. *Advances in neural information processing systems*, 34:8780–8794, 2021. 4
- [9] Siyuan Fan, Wenke Huang, Xiantao Cai, and Bo Du. 3d human interaction generation: A survey. *arXiv preprint arXiv:2503.13120*, 2025. 3
- [10] Mihai Fieraru, Mihai Zanfir, Elisabeta Oneata, Alin-Ionut Popa, Vlad Olaru, and Cristian Sminchisescu. Three-dimensional reconstruction of human interactions. In *Proceedings of the IEEE/CVF Conference on Computer Vision and Pattern Recognition*, pages 7214–7223, 2020. 2, 3
- [11] Anindita Ghosh, Rishabh Dabral, Vladislav Golyanik, Christian Theobalt, and Philipp Slusallek. Remos: 3d motion-conditioned reaction synthesis for two-person interactions. In *European Conference on Computer Vision (ECCV)*, 2024. 2
- [12] Chuan Guo, Xinxin Zuo, Sen Wang, Shihao Zou, Qingyao Sun, Annan Deng, Minglun Gong, and Li Cheng. Action2motion: Conditioned generation of 3d human motions. In *Proceedings of the 28th ACM international conference on multimedia*, pages 2021–2029, 2020. 2
- [13] Chuan Guo, Shihao Zou, Xinxin Zuo, Sen Wang, Wei Ji, Xingyu Li, and Li Cheng. Generating diverse and natural 3d human motions from text. In *Proceedings of the IEEE/CVF conference on computer vision and pattern recognition*, pages 5152–5161, 2022. 2, 6, 7, 12, 13, 14
- [14] Chuan Guo, Xinxin Zuo, Sen Wang, and Li Cheng. Tm2t: Stochastic and tokenized modeling for the reciprocal generation of 3d human motions and texts. In *European Conference on Computer Vision*, pages 580–597. Springer, 2022. 3
- [15] Chuan Guo, Yuxuan Mu, Muhammad Gohar Javed, Sen Wang, and Li Cheng. Momask: Generative masked modeling of 3d human motions. In *Proceedings of the IEEE/CVF Conference on Computer Vision and Pattern Recognition*, pages 1900–1910, 2024. 2, 3
- [16] Debanu Gupta, Shubh Maheshwari, Sai Shashank Kalakonda, Manasvi, and Ravi Kiran Sarvadevabhatla. Dsg: A scalable deep framework for action-conditioned multi-actor full body motion synthesis. In *Proceedings of the IEEE/CVF Winter Conference on Applications of Computer Vision (WACV)*, 2023. 2
- [17] Yiheng Huang, Hui Yang, Chuanchen Luo, Yuxi Wang, Shibiao Xu, Zhaoxiang Zhang, Man Zhang, and Junran Peng. Stablemofusion: Towards robust and efficient diffusion-based motion generation framework. In *Proceedings of the 32nd ACM International Conference on Multimedia*, pages 224–232, 2024. 2
- [18] Catalin Ionescu, Dragos Papava, Vlad Olaru, and Cristian Sminchisescu. Human3.6m: Large scale datasets and predictive methods for 3d human sensing in natural environments. *IEEE Transactions on Pattern Analysis and Machine Intelligence*, 36(7):1325–1339, 2014. 2
- [19] Muhammad Gohar Javed, Chuan Guo, Li Cheng, and Xingyu Li. Intermask: 3d human interaction generation via collaborative masked modeling. *arXiv preprint arXiv:2410.10010*, 2024. 3, 7, 12, 14
- [20] Kaiyang Ji, Ye Shi, Zichen Jin, Kangyi Chen, Lan Xu, Yuexin Ma, Jingyi Yu, and Jingya Wang. Towards immersive human-x interaction: A real-time framework for physically plausible motion synthesis. In *Proceedings of the IEEE/CVF International Conference on Computer Vision*, pages 10173–10183, 2025. 3
- [21] Biao Jiang, Xin Chen, Wen Liu, Jingyi Yu, Gang Yu, and Tao Chen. Motiongpt: Human motion as a foreign language. *Advances in Neural Information Processing Systems*, 36:20067–20079, 2023. 3
- [22] Jihoon Kim, Jiseob Kim, and Sungjoon Choi. Flame: Free-form language-based motion synthesis & editing. In *Pro-*

- ceedings of the AAAI Conference on Artificial Intelligence, pages 8255–8263, 2023. 2
- [23] Han Liang, Wenqian Zhang, Wenxuan Li, Jingyi Yu, and Lan Xu. Intergen: Diffusion-based multi-human motion generation under complex interactions. *International Journal of Computer Vision*, 132(9):3463–3483, 2024. 2, 3, 4, 7, 12, 14
- [24] Jiaheng Liu, Dawei Zhu, Zhiqi Bai, Yancheng He, Huanxuan Liao, Haoran Que, Zekun Wang, Chenchen Zhang, Ge Zhang, Jiebin Zhang, et al. A comprehensive survey on long context language modeling. *arXiv preprint arXiv:2503.17407*, 2025. 7
- [25] Matthew Loper, Naureen Mahmood, Javier Romero, Gerard Pons-Moll, and Michael J. Black. SMPL: A skinned multi-person linear model. *ACM Trans. Graphics (Proc. SIGGRAPH Asia)*, 34(6):248:1–248:16, 2015. 2, 13
- [26] Naureen Mahmood, Nima Ghorbani, Nikolaus F. Troje, Gerard Pons-Moll, and Michael J. Black. AMASS: Archive of motion capture as surface shapes. In *International Conference on Computer Vision*, pages 5442–5451, 2019. 2
- [27] Zichong Meng, Zeyu Han, Xiaogang Peng, Yiming Xie, and Huaizu Jiang. Absolute coordinates make motion generation easy. *arXiv preprint arXiv:2505.19377*, 2025. 2, 3
- [28] Zichong Meng, Yiming Xie, Xiaogang Peng, Zeyu Han, and Huaizu Jiang. Rethinking diffusion for text-driven human motion generation: Redundant representations, evaluation, and masked autoregression. In *Proceedings of the Computer Vision and Pattern Recognition Conference*, pages 27859–27871, 2025. 3, 6, 13
- [29] Evonne Ng, Donglai Xiang, Hanbyul Joo, and Kristen Grauman. You2me: Inferring body pose in egocentric video via first and second person interactions. *CVPR*, 2020. 2, 3
- [30] Georgios Pavlakos, Vasileios Choutas, Nima Ghorbani, Timo Bolkart, Ahmed A. A. Osman, Dimitrios Tzionas, and Michael J. Black. Expressive body capture: 3D hands, face, and body from a single image. In *Proceedings IEEE Conf. on Computer Vision and Pattern Recognition (CVPR)*, pages 10975–10985, 2019. 2, 3, 12
- [31] Ekkasit Pinyoanuntapong, Pu Wang, Minwoo Lee, and Chen Chen. Mmm: Generative masked motion model. In *Proceedings of the IEEE/CVF Conference on Computer Vision and Pattern Recognition*, pages 1546–1555, 2024. 3
- [32] Matthias Plappert, Christian Mandery, and Tamim Asfour. The KIT motion-language dataset. *Big Data*, 4(4):236–252, 2016. 2
- [33] Abhinanda R. Punnakkal, Arjun Chandrasekaran, Nikos Athanasiou, Alejandra Quiros-Ramirez, and Michael J. Black. BABEL: Bodies, action and behavior with english labels. In *Proceedings IEEE/CVF Conf. on Computer Vision and Pattern Recognition (CVPR)*, pages 722–731, 2021. 2
- [34] Aditya Ramesh, Prafulla Dhariwal, Alex Nichol, Casey Chu, and Mark Chen. Hierarchical text-conditional image generation with clip latents. *arXiv preprint arXiv:2204.06125*, 1(2):3, 2022. 4
- [35] Pablo Ruiz-Ponce, German Barquero, Cristina Palmero, Sergio Escalera, and José García-Rodríguez. in2in: Leveraging individual information to generate human interactions. In *Proceedings of the IEEE/CVF Conference on Computer Vision and Pattern Recognition*, pages 1941–1951, 2024. 3, 4, 6
- [36] Pablo Ruiz-Ponce, German Barquero, Cristina Palmero, Sergio Escalera, and José García-Rodríguez. Mixermdm: Learnable composition of human motion diffusion models. In *Proceedings of the Computer Vision and Pattern Recognition Conference*, pages 12380–12390, 2025. 2, 4
- [37] Yonatan Shafir, Guy Tevet, Roy Kapon, and Amit H Bermano. Human motion diffusion as a generative prior. *arXiv preprint arXiv:2303.01418*, 2023. 3
- [38] Amir Shahroudy, Jun Liu, Tian-Tsong Ng, and Gang Wang. Ntu rgb+ d: A large scale dataset for 3d human activity analysis. In *Proceedings of the IEEE conference on computer vision and pattern recognition*, pages 1010–1019, 2016. 2
- [39] Yi Shi, Jingbo Wang, Xuekun Jiang, Bingkun Lin, Bo Dai, and Xue Bin Peng. Interactive character control with autoregressive motion diffusion models. *ACM Transactions on Graphics (TOG)*, 43(4):1–14, 2024. 3
- [40] Kewei Sui, Anindita Ghosh, Inwoo Hwang, Bing Zhou, Jian Wang, and Chuan Guo. A survey on human interaction motion generation. *arXiv preprint arXiv:2503.12763*, 2025. 3
- [41] Julian Tanke, Linguang Zhang, Amy Zhao, Chengcheng Tang, Yujun Cai, Lezi Wang, Po-Chen Wu, Juergen Gall, and Cem Keskin. Social diffusion: Long-term multiple human motion anticipation. In *Proceedings of the IEEE/CVF International Conference on Computer Vision*, pages 9601–9611, 2023. 2, 3
- [42] Julian Tanke, Takashi Shibuya, Kengo Uchida, Koichi Saito, and Yuki Mitsufuji. Dyadic mamba: Long-term dyadic human motion synthesis. In *Proceedings of the Computer Vision and Pattern Recognition Conference*, pages 2868–2877, 2025. 3
- [43] Guy Tevet, Brian Gordon, Amir Hertz, Amit H Bermano, and Daniel Cohen-Or. Motionclip: Exposing human motion generation to clip space. In *European Conference on Computer Vision*, pages 358–374. Springer, 2022. 2
- [44] Guy Tevet, Sigal Raab, Brian Gordon, Yoni Shafir, Daniel Cohen-or, and Amit Haim Bermano. Human motion diffusion model. In *The Eleventh International Conference on Learning Representations*, 2023. 2, 3, 4
- [45] Guy Tevet, Sigal Raab, Setareh Cohan, Daniele Reda, Zhengyi Luo, Xue Bin Peng, Amit Haim Bermano, and Michiel van de Panne. CLoSD: Closing the loop between simulation and diffusion for multi-task character control. In *The Thirteenth International Conference on Learning Representations*, 2025. 3, 5
- [46] NP Van der Aa, Xinghan Luo, Geert-Jan Giezeman, Robby T Tan, and Remco C Veltkamp. Umpm benchmark: A multi-person dataset with synchronized video and motion capture data for evaluation of articulated human motion and interaction. In *2011 IEEE international conference on computer vision workshops (ICCV Workshops)*, pages 1264–1269. IEEE, 2011. 2, 3
- [47] Zhenzhi Wang, Jingbo Wang, Yixuan Li, Dahua Lin, and Bo Dai. Intercontrol: Zero-shot human interaction generation by controlling every joint. *Advances in Neural Information Processing Systems*, 37:105397–105424, 2024. 3

- [48] Guo Wen, Bie Xiaoyu, Alameda-Pineda Xavier, and Moreno-Noguer Francesc. Multi-person extreme motion prediction. In *Proceedings of the IEEE International Conference on Computer Vision and Pattern Recognition (CVPR)*, 2022. 2, 3
- [49] Lixing Xiao, Shunlin Lu, Huaijin Pi, Ke Fan, Liang Pan, Yueer Zhou, Ziyong Feng, Xiaowei Zhou, Sida Peng, and Jingbo Wang. Motionstreamer: Streaming motion generation via diffusion-based autoregressive model in causal latent space. *arXiv preprint arXiv:2503.15451*, 2025. 3
- [50] Zhisheng Xiao, Karsten Kreis, and Arash Vahdat. Tackling the generative learning trilemma with denoising diffusion GANs. In *International Conference on Learning Representations (ICLR)*, 2022. 4
- [51] Linfeng Xu, Qingbo Wu, Lili Pan, Fanman Meng, Hongliang Li, Chiyuan He, Hanxin Wang, Shaoxu Cheng, and Yu Dai. Towards continual egocentric activity recognition: A multi-modal egocentric activity dataset for continual learning. *IEEE Transactions on Multimedia*, 26:2430–2443, 2023. 2
- [52] Liang Xu, Xintao Lv, Yichao Yan, Xin Jin, Shuwen Wu, Congsheng Xu, Yifan Liu, Yizhou Zhou, Fengyun Rao, Xingdong Sheng, et al. Inter-x: Towards versatile human-human interaction analysis. In *Proceedings of the IEEE/CVF conference on computer vision and pattern recognition*, pages 22260–22271, 2024. 2, 3, 6, 12
- [53] Wenning Xu, Shiyu Fan, Paul Henderson, and Edmond SL Ho. Multi-person interaction generation from two-person motion priors. In *Proceedings of the Special Interest Group on Computer Graphics and Interactive Techniques Conference Conference Papers*, pages 1–11, 2025. 3, 14
- [54] Yifei Yin, Chen Guo, Manuel Kaufmann, Juan Zarate, Jie Song, and Otmar Hilliges. Hi4d: 4d instance segmentation of close human interaction. In *Computer Vision and Pattern Recognition (CVPR)*, 2023. 2, 3
- [55] Heng Yu, Juze Zhang, Changan Chen, Tiange Xiang, Yusu Fang, Juan Carlos Niebles, and Ehsan Adeli. Socialgen: Modeling multi-human social interaction with language models. *arXiv preprint arXiv:2503.22906*, 2025. 2, 3
- [56] Weihao Yuan, Yisheng He, Weichao Shen, Yuan Dong, Xiaodong Gu, Zilong Dong, Liefeng Bo, and Qixing Huang. Mogents: Motion generation based on spatial-temporal joint modeling. *Advances in Neural Information Processing Systems*, 37:130739–130763, 2024. 3
- [57] Ye Yuan, Jiaming Song, Umar Iqbal, Arash Vahdat, and Jan Kautz. Physdiff: Physics-guided human motion diffusion model. In *Proceedings of the IEEE/CVF international conference on computer vision*, pages 16010–16021, 2023. 2
- [58] Jianrong Zhang, Yangsong Zhang, Xiaodong Cun, Yong Zhang, Hongwei Zhao, Hongtao Lu, Xi Shen, and Ying Shan. Generating human motion from textual descriptions with discrete representations. In *Proceedings of the IEEE/CVF conference on computer vision and pattern recognition*, pages 14730–14740, 2023. 3
- [59] Mingyuan Zhang, Xinying Guo, Liang Pan, Zhongang Cai, Fangzhou Hong, Huirong Li, Lei Yang, and Ziwei Liu. Remodiffuse: Retrieval-augmented motion diffusion model. In *Proceedings of the IEEE/CVF International Conference on Computer Vision*, pages 364–373, 2023. 2
- [60] Mingyuan Zhang, Zhongang Cai, Liang Pan, Fangzhou Hong, Xinying Guo, Lei Yang, and Ziwei Liu. Motiandiffuse: Text-driven human motion generation with diffusion model. *IEEE transactions on pattern analysis and machine intelligence*, 46(6):4115–4128, 2024. 2
- [61] Yaqi Zhang, Di Huang, Bin Liu, Shixiang Tang, Yan Lu, Lu Chen, Lei Bai, Qi Chu, Nenghai Yu, and Wanli Ouyang. Motiongpt: Finetuned llms are general-purpose motion generators. In *Proceedings of the AAAI Conference on Artificial Intelligence*, pages 7368–7376, 2024. 3
- [62] Yan Zhang, Yao Feng, Alpár Cseke, Nitin Saini, Nathan Bajandas, Nicolas Heron, and Michael J. Black. Primal: Physically reactive and interactive motor model for avatar learning, 2025. 3, 5
- [63] Kaifeng Zhao, Gen Li, and Siyu Tang. Dartcontrol: A diffusion-based autoregressive motion model for real-time text-driven motion control. *arXiv preprint arXiv:2410.05260*, 2024. 3
- [64] Chongyang Zhong, Lei Hu, Zihao Zhang, and Shihong Xia. Attt2m: Text-driven human motion generation with multi-perspective attention mechanism. In *Proceedings of the IEEE/CVF international conference on computer vision*, pages 509–519, 2023. 3
- [65] Wenyang Zhou, Zhiyang Dou, Zeyu Cao, Zhouyingcheng Liao, Jingbo Wang, Wenjia Wang, Yuan Liu, Taku Komura, Wenping Wang, and Lingjie Liu. Emdm: Efficient motion diffusion model for fast and high-quality motion generation. In *European Conference on Computer Vision*, pages 18–38. Springer, 2024. 2
- [66] Yi Zhou, Connelly Barnes, Jingwan Lu, Jimei Yang, and Hao Li. On the continuity of rotation representations in neural networks. In *Proceedings of the IEEE/CVF conference on computer vision and pattern recognition*, pages 5745–5753, 2019. 3
- [67] Wentao Zhu, Xiaoxuan Ma, Dongwoo Ro, Hai Ci, Jinlu Zhang, Jiabin Shi, Feng Gao, Qi Tian, and Yizhou Wang. Human motion generation: A survey. *IEEE Transactions on Pattern Analysis and Machine Intelligence*, 46(4):2430–2449, 2023. 1, 2

Interact2Ar: Full-Body Human-Human Interaction Generation via Autoregressive Diffusion Models Supplementary Material

This supplementary material aims to enhance the reproducibility and understanding of the work contributions. In Sec. A, we outline the implementation details of the state-of-the-art models used for comparison, provide detailed formulations of the loss functions employed in training, describe the newly proposed body-part-specific evaluators, detail the user study methodology, and explain the implementation of adaptive interaction capabilities. In Sec. B, we complement the quantitative evaluation with results using the original evaluators from the Inter-X dataset and present an extended ablation study examining different memory configurations across all evaluation settings. In Sec. C, we describe the accompanying Supplementary Video, which includes additional visual examples and side-by-side comparisons with previous state-of-the-art methods to better illustrate the Interact2Ar capabilities. Finally, in Sec. D, we detail the code and data availability to ensure full reproducibility of our work.

A. Implementation Details

A.1. State-of-the-art Implementations

We compared Interact2Ar with previous SOTA methods on the Inter-X dataset. We primarily compared against T2M [13], InterGen [23], and InterMask [19].

InterGen is the state-of-the-art baseline among the original baselines proposed by the Inter-X [52] dataset authors. However, given that the weights are not public, we re-trained InterGen using the original implementation details described in the paper, including a transformer encoder with 8 blocks and 8 heads (latent dimension 512, feed-forward dimension 1024). The model uses 1000 steps with DDIM-50 sampling and was trained for 5000 epochs using EMA and AdamW. Following Inter-X we used a learning rate 1×10^{-4} with weight decay 2×10^{-5} and a batch size of 128. Given that the motion representation that we use is not the same as in the InterHuman dataset [23], we used our loss adaptations using forward kinematics to train the model.

A.2. Losses

In this section, we provide detailed formulations and explanations for each component of our training loss function.

Representation Loss. The representation loss $\mathcal{L}_{\text{repr}}$ directly measures the ℓ_2 distance between the predicted and ground truth SMPL-X parameters [30] in their raw representation space:

$$\mathcal{L}_{\text{repr}}(x, \hat{x}) = \|x - \hat{x}\|_2^2, \quad (8)$$

where $x \in \mathbb{R}^{T \times D}$ represents the ground truth SMPL-X parameters across T frames with dimensionality D , and \hat{x} denotes the predicted parameters. This loss operates directly on the body pose parameters, hand articulations, and global trajectory, providing a direct supervision signal in the learned representation space.

Root Orientation Loss. The root orientation loss $\mathcal{L}_{\text{orient}}$ specifically penalizes errors in the global root orientation of each individual:

$$\mathcal{L}_{\text{orient}}(r, \hat{r}) = \|r_a - \hat{r}_a\|_2^2 + \|r_b - \hat{r}_b\|_2^2, \quad (9)$$

where $r_a, r_b \in \mathbb{R}^{T \times 3}$ represent the ground truth root orientations for individuals a and b respectively, and \hat{r}_a, \hat{r}_b are the corresponding predictions. This loss ensures that the global facing direction and body orientation of each person are accurately captured, which is crucial for modeling proper spatial relationships in interactions.

A.2.1. Kinematic Losses

We compute the following geometric losses through forward kinematics (FK), which converts SMPL-X parameters to 3D joint positions: $p = \text{FK}(x)$.

Joint Position Loss. The global joint position loss \mathcal{L}_{pos} penalizes discrepancies in the predicted 3D locations of body joints:

$$\mathcal{L}_{\text{pos}}(p, \hat{p}) = \|p_a - \hat{p}_a\|_2^2 + \|p_b - \hat{p}_b\|_2^2, \quad (10)$$

where $p_a, p_b \in \mathbb{R}^{T \times N_j \times 3}$ are the ground truth global joint positions for both individuals with N_j joints per person, and \hat{p}_a, \hat{p}_b are the corresponding predicted positions. This loss enforces spatial accuracy in the generated motions.

Joint Velocity Loss. To promote temporal smoothness and physical plausibility, we apply a velocity loss on the joint positions:

$$\mathcal{L}_{\text{vel}}(v, \hat{v}) = \|v_a - \hat{v}_a\|_2^2 + \|v_b - \hat{v}_b\|_2^2, \quad (11)$$

where $v_t = p_t - p_{t-1}$ represents the joint velocities computed as the difference between consecutive frames. This loss discourages unnatural jittering and encourages smooth, realistic motion trajectories.

Foot Contact Loss. The foot contact loss $\mathcal{L}_{\text{foot}}$ reduces artifacts such as foot skating and floating:

$$\mathcal{L}_{\text{foot}}(f, \hat{f}) = \sum_{i \in \{\text{feet}\}} \|v_i \odot f_i\|_2^2 + \|\hat{v}_i \odot \hat{f}_i\|_2^2, \quad (12)$$

where v_i denotes the velocity of foot joint i , $f_i \in \{0, 1\}^T$ is a binary contact indicator (1 when the foot is in contact

with the ground, 0 otherwise), and \odot represents element-wise multiplication. This loss penalizes foot motion when contact is detected, enforcing physical constraints.

Pairwise Joint Distance Map Loss. To capture the fine-grained spatial relationships between the two individuals, we introduce the distance map loss $\mathcal{L}_{\text{dist}}$:

$$\mathcal{L}_{\text{dist}}(d, \hat{d}) = \|(D(p_a, p_b) - D(\hat{p}_a, \hat{p}_b)) \odot M\|_2^2, \quad (13)$$

where $D(p_a, p_b) \in \mathbb{R}^{T \times N_j \times N_j}$ computes the pairwise Euclidean distance between all joints of individual a and all joints of individual b :

$$D(p_a, p_b)_{i,j} = \|p_a^{(i)} - p_b^{(j)}\|_2, \quad (14)$$

with $p_a^{(i)}$ and $p_b^{(j)}$ denoting the positions of the i -th joint of person a and j -th joint of person b , respectively. The binary mask $M \in \{0, 1\}^{T \times N_j \times N_j}$ activates the loss only for joint pairs in close proximity in the ground truth, focusing supervision on spatial relationships that are most critical for realistic interactions. This ensures that the spatial proximity patterns between the two individuals match the ground truth, which is essential for generating realistic interactive behaviors such as handshakes, hugs, and other contact-based interactions.

Loss Weighting. The weighting coefficients $\{\lambda_{\text{repr}}, \lambda_{\text{orient}}, \lambda_{\text{pos}}, \lambda_{\text{vel}}, \lambda_{\text{foot}}, \lambda_{\text{dist}}\}$ are determined through grid search to balance the contribution of each loss term. These weights are calibrated to normalize the magnitude differences across loss components, ensuring that each term contributes meaningfully to the optimization process. The specific values used in our experiments are: $\lambda_{\text{repr}} = 1.0$, $\lambda_{\text{orient}} = 0.1$, $\lambda_{\text{pos}} = 1.0$, $\lambda_{\text{vel}} = 1.0$, $\lambda_{\text{foot}} = 1.0$, and $\lambda_{\text{dist}} = 0.5$.

A.3. Evaluators

Sec. 4 introduced an improved evaluation pipeline over the original evaluator provided on the Inter-X dataset. This new pipeline better assesses interaction quality and provides more granular information. To achieve this, we introduced a set of new body-part-specific evaluators retrained to have deeper knowledge of the global information of the interactants.

For all evaluators, we used the architecture proposed in [13], where a motion and a text feature extractor are trained via contrastive learning, and these encoded representations are used to calculate the remaining metrics. Using this architecture, we trained 3 evaluators for 300 epochs at a learning rate of 1×10^{-4} to generate feature vectors of size 512. The full evaluator was trained using information from all SMPL-X joints, the body evaluator using only the base SMPL [25] joints, and the hand evaluator using the additional 30 joints used for hands.

We additionally made the evaluators more robust, as demonstrated in Tab. 1 Based on the findings of [28], we decided to train an evaluator using only joint positions. Since the positioning between different individuals has great importance for interactions, we represented joint positions using global coordinates. These coordinates are calculated using a forward kinematic function on SMPL-X rotations predicted by our model.

A.4. User Study

The user study was performed with 35 different participants to rank 10 different interactions extracted from: ground truth, our model, InterMask, and InterGen. The 35 participants were in the range of 25 to 55 years old, from different nationalities, all having higher degrees of study (bachelor’s or more). Among the participants, there was a similar distribution of individuals familiarized with the human motion generation task and not. Fig. A presents a real frame from one of the videos that the users had to rank. In the video, there is a textual description at the top, and there are 4 videos randomly shuffled for each of the possible options. From each video, the participant had to rank each interaction based on the alignment with the textual description and the quality of the hand generation. We also included the ground truth provided by the dataset for this textual description, so the user always had an aligned interaction with the text and could rank all videos based on the overall quality. To ensure even distribution of the interaction motions, all the textual descriptions were extracted from the test set, and every one pertained to a different action category.

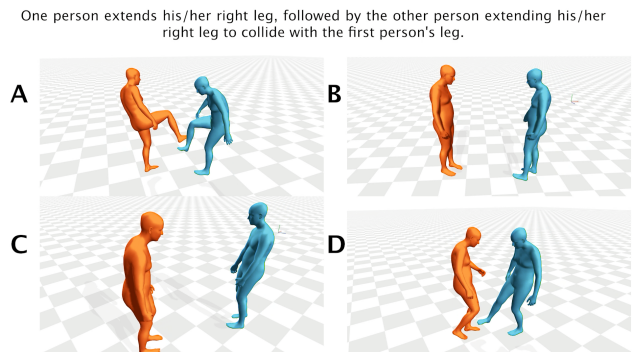


Figure A. **User study.** A sample of the user study where 35 participants evaluated and ranked the text alignment and the hand quality of Interact2Ar and baseline methods.

A.5. Adaptive Interactions

Temporal Motion Composition. We implement this with a large context window that includes all previously generated actions. Given the Mixed Memory approach we proposed, the memory buffer \mathcal{M} accesses this information and

	Methods	R-Precision \uparrow			FID \downarrow	MM Dist \downarrow	Diversity \rightarrow	MModality \uparrow	PJ \uparrow	AUJ \downarrow
		Top 1	Top 2	Top 3						
Full	<i>Ground Truth</i>	0.429 \pm .00	0.626 \pm .00	0.736 \pm .00	0.002 \pm .00	3.536 \pm .01	9.734 \pm .08	–	0.021 \pm .00	3.944 \pm .00
	T2M [13]	0.184 \pm .01	0.298 \pm .01	0.396 \pm .01	5.481 \pm .38	9.576 \pm .01	2.771 \pm .15	2.761 \pm .04	1.889 \pm .12	124.9 \pm 1.9
	InterGen [23]	0.327 \pm .00	0.506 \pm .00	0.619 \pm .00	2.601 \pm .10	4.580 \pm .02	9.200 \pm .11	3.999 \pm .11	2.132 \pm .12	84.16 \pm 3.1
	InterMask [19]	0.403 \pm .01	0.595 \pm .00	0.705 \pm .01	0.399 \pm .01	3.705 \pm .02	9.046 \pm .07	2.261 \pm .08	2.328 \pm .21	61.74 \pm .50
	Interact2Ar*	0.433 \pm .00	0.623 \pm .00	0.727 \pm .00	0.255 \pm .01	3.618 \pm .01	9.066 \pm .07	2.820 \pm .08	2.110 \pm .12	54.97 \pm .67
	Interact2Ar	0.441 \pm .00	0.631 \pm .00	0.737 \pm .00	0.148 \pm .01	3.581 \pm .01	9.147 \pm .06	1.529 \pm .05	0.136 \pm .00	8.837 \pm .17
Body	<i>Ground Truth</i>	0.431 \pm .00	0.621 \pm .00	0.725 \pm .00	0.002 \pm .00	3.371 \pm .01	8.931 \pm .06	–	0.014 \pm .00	3.832 \pm .00
	T2M [13]	0.310 \pm .00	0.468 \pm .00	0.570 \pm .00	3.346 \pm .05	4.465 \pm .02	8.113 \pm .09	0.604 \pm .03	1.857 \pm .10	115.6 \pm 1.7
	InterGen [23]	0.349 \pm .00	0.528 \pm .00	0.637 \pm .00	1.708 \pm .05	4.363 \pm .02	9.253 \pm .09	3.596 \pm .11	2.116 \pm .13	77.09 \pm 3.9
	InterMask [19]	0.401 \pm .00	0.594 \pm .00	0.707 \pm .00	0.741 \pm .03	3.483 \pm .01	8.915 \pm .08	1.589 \pm .05	2.549 \pm .16	59.41 \pm .69
	Interact2Ar*	0.447 \pm .00	0.643 \pm .00	0.750 \pm .00	0.273 \pm .02	3.231 \pm .01	9.074 \pm .08	2.347 \pm .08	2.040 \pm .17	53.30 \pm .51
	Interact2Ar	0.446 \pm .00	0.639 \pm .00	0.744 \pm .00	0.212 \pm .01	3.287 \pm .02	9.055 \pm .08	1.470 \pm .05	0.123 \pm .00	6.620 \pm .13
Hands	<i>Ground Truth</i>	0.372 \pm .00	0.556 \pm .00	0.663 \pm .00	0.002 \pm .00	3.893 \pm .01	8.611 \pm .07	–	0.017 \pm .00	2.480 \pm .00
	T2M [13]	0.325 \pm .00	0.486 \pm .00	0.590 \pm .00	2.114 \pm .05	4.296 \pm .02	8.129 \pm .06	0.595 \pm .04	1.767 \pm .09	113.1 \pm 1.9
	InterGen [23]	0.331 \pm .00	0.504 \pm .00	0.617 \pm .00	4.664 \pm .19	4.560 \pm .03	9.654 \pm .12	4.155 \pm .12	2.049 \pm .12	70.47 \pm 2.9
	InterMask [19]	0.380 \pm .00	0.568 \pm .00	0.681 \pm .00	0.383 \pm .02	3.729 \pm .02	8.689 \pm .08	1.883 \pm .09	2.201 \pm .16	59.77 \pm .76
	Interact2Ar*	0.402 \pm .00	0.592 \pm .00	0.704 \pm .00	0.242 \pm .01	3.639 \pm .02	8.972 \pm .08	2.877 \pm .08	1.923 \pm .09	51.03 \pm .49
	Interact2Ar	0.393 \pm .00	0.584 \pm .00	0.695 \pm .00	0.238 \pm .01	3.711 \pm .01	8.853 \pm .07	1.754 \pm .05	0.120 \pm .00	7.474 \pm .16

Table A. Comparison of our model (Interact2Ar) to the state of the art in human-human interaction motion generation on the Inter-X dataset. *Interact2Ar model is the version without autoregressive generation. All evaluations have been executed 20 times to elude the randomness of the generation. \pm indicates the 95% confidence interval. We highlight the **best** and the second best results.

enables Interact2Ar to generate seamless transitions while accounting for the complete action history.

Real-Time Disturbance Adaptation. To effectively assess the real-time adaptation of Interact2Ar, we randomly translated one individual in the XZ plane between different sub-motion generations. This simulates noisy contexts and disturbances produced by the environment or other individuals. Traditional diffusion models and Masked VQ-VAE Transformers, such as InterMask, cannot enable this capability because they produce the whole sequence at once, preventing adaptation until the entire motion is generated.

Sequential Multi-Person Interactions. We implemented this using two couples performing 2 different actions with their respective memories. Once they finish their actions, we take one individual from each couple and generate a new interaction with the newly formed couple. For the memories, we retain the original memories from the initial couples and create a new memory using information from the new couple. This enables seamless interaction while maintaining access to previously performed actions. While this implementation only generates sequential multi-human interactions, the idea can be expanded to generate parallel multi-human interactions as proposed in [53].

B. Quantitative Evaluation

B.1. Original Evaluators

In Tab. 1, we present a quantitative evaluation of the robustness of our newly proposed evaluators with respect to the

original ones provided in the Inter-X dataset. Additionally, we provide the main metrics of our model in Tab. 2 using those newly trained evaluators. In Tab. A, we performed the same evaluation using the original full-body evaluator trained directly with the SMPL-X representation, alongside body- and hand-specific evaluators using the same representation. We can observe in this case that Interact2Ar still outperforms previous methods. However, these differences are not as large as when using our evaluators. It can even be observed that in the body- and hand-specific evaluators, the non-autoregressive version of Interact2Ar obtains slightly better metrics than the autoregressive one. These smaller differences occur because rotation-based evaluators penalize diffusion models compared to VQ-VAE approaches. Furthermore, the original evaluators do not account for degradations in the global positioning of the individuals, which makes them incapable of detecting small differences, such as those between the autoregressive and non-autoregressive versions.

B.2. Extended Ablation

In Tab. 3, we present an extended ablation study where different memory configurations have been tested to determine which provides the best trade-off between quality in terms of metrics and memory size. Tab. B is an extended version of this ablation where all the different evaluators have been used. As can be observed, the overall tendency that we observed for the full evaluator remains consistent in the body and hands evaluators. While adding more memory can re-

	Method	m_s	m_l	\mathcal{M}	R-Precision \uparrow			FID \downarrow	MM Dist \downarrow	Diversity \rightarrow	MModality \uparrow
					Top 1	Top 2	Top 3				
Full	<i>Ground Truth</i>	-	-	-	0.431 \pm .00	0.631 \pm .00	0.740 \pm .00	0.002 \pm .00	3.318 \pm .01	8.973 \pm .10	-
	Interact2Ar Regular Memory	15	-	15	0.449 \pm .00	0.653 \pm .00	0.765 \pm .00	0.283 \pm .01	3.141 \pm .01	9.275 \pm .08	1.491 \pm .05
		30	-	30	0.445 \pm .00	0.656 \pm .00	0.769 \pm .00	0.346 \pm .01	3.122 \pm .01	9.240 \pm .06	1.471 \pm .04
		60	-	60	0.458 \pm .00	0.665 \pm .00	0.776 \pm .00	0.316 \pm .01	3.071 \pm .02	9.285 \pm .07	1.394 \pm .06
		90	-	90	0.452 \pm .00	0.660 \pm .01	0.771 \pm .00	0.412 \pm .01	3.103 \pm .01	9.264 \pm .07	1.344 \pm .04
		120	-	120	0.456 \pm .00	0.665 \pm .00	0.774 \pm .00	0.413 \pm .01	3.084 \pm .01	9.299 \pm .07	1.336 \pm .04
	Interact2Ar Mixed Memory	15	15	18	0.448 \pm .00	0.655 \pm .00	0.769 \pm .00	0.289 \pm .01	3.131 \pm .01	9.255 \pm .06	1.461 \pm .05
		15	45	24	0.453 \pm .00	0.661 \pm .00	0.773 \pm .00	0.277 \pm .01	3.095 \pm .01	9.305 \pm .07	1.427 \pm .04
		15	75	30	0.453 \pm .00	0.661 \pm .00	0.771 \pm .00	0.279 \pm .01	3.110 \pm .01	9.318 \pm .06	1.346 \pm .05
		15	105	36	0.458 \pm .00	0.664 \pm .00	0.773 \pm .00	0.325 \pm .01	3.089 \pm .01	9.346 \pm .06	1.363 \pm .04
	Body	<i>Ground Truth</i>	-	-	-	0.462 \pm .01	0.655 \pm .00	0.758 \pm .00	0.001 \pm .00	3.272 \pm .01	9.002 \pm .07
Interact2Ar Regular Memory		15	-	15	0.466 \pm .00	0.667 \pm .00	0.774 \pm .00	0.399 \pm .01	3.194 \pm .02	9.319 \pm .09	1.483 \pm .05
		30	-	30	0.471 \pm .00	0.672 \pm .00	0.780 \pm .00	0.428 \pm .01	3.168 \pm .01	9.195 \pm .06	1.439 \pm .05
		60	-	60	0.474 \pm .01	0.677 \pm .00	0.781 \pm .00	0.397 \pm .01	3.158 \pm .01	9.244 \pm .08	1.388 \pm .05
		90	-	90	0.471 \pm .00	0.678 \pm .00	0.781 \pm .00	0.475 \pm .01	3.188 \pm .01	9.260 \pm .07	1.337 \pm .04
		120	-	120	0.470 \pm .00	0.676 \pm .00	0.781 \pm .00	0.463 \pm .01	3.168 \pm .01	9.311 \pm .07	1.304 \pm .04
Interact2Ar Mixed Memory		15	15	18	0.471 \pm .00	0.676 \pm .00	0.780 \pm .00	0.354 \pm .01	3.169 \pm .01	9.268 \pm .07	1.442 \pm .04
		15	45	24	0.469 \pm .00	0.672 \pm .00	0.779 \pm .00	0.352 \pm .01	3.173 \pm .01	9.271 \pm .08	1.421 \pm .04
		15	75	30	0.474 \pm .00	0.673 \pm .00	0.778 \pm .00	0.331 \pm .01	3.175 \pm .01	9.276 \pm .06	1.362 \pm .05
		15	105	36	0.477 \pm .00	0.678 \pm .00	0.782 \pm .00	0.411 \pm .01	3.141 \pm .01	9.321 \pm .06	1.343 \pm .04
Hands		<i>Ground Truth</i>	-	-	-	0.399 \pm .00	0.597 \pm .00	0.713 \pm .00	0.002 \pm .00	3.312 \pm .01	8.370 \pm .05
	Interact2Ar Regular Memory	15	-	15	0.414 \pm .00	0.620 \pm .00	0.734 \pm .00	0.206 \pm .01	3.165 \pm .01	8.580 \pm .07	1.540 \pm .06
		30	-	30	0.420 \pm .01	0.627 \pm .00	0.744 \pm .00	0.302 \pm .01	3.129 \pm .01	8.515 \pm .07	1.495 \pm .06
		60	-	60	0.425 \pm .00	0.630 \pm .00	0.748 \pm .00	0.273 \pm .01	3.112 \pm .01	8.595 \pm .07	1.405 \pm .06
		90	-	90	0.423 \pm .01	0.630 \pm .01	0.747 \pm .00	0.350 \pm .01	3.126 \pm .01	8.607 \pm .07	1.354 \pm .05
		120	-	120	0.424 \pm .00	0.634 \pm .01	0.748 \pm .00	0.378 \pm .01	3.111 \pm .01	8.589 \pm .08	1.370 \pm .05
	Interact2Ar Mixed Memory	15	15	18	0.421 \pm .00	0.628 \pm .00	0.743 \pm .00	0.258 \pm .01	3.135 \pm .01	8.551 \pm .08	1.504 \pm .06
		15	45	24	0.422 \pm .00	0.629 \pm .00	0.745 \pm .00	0.257 \pm .01	3.111 \pm .01	8.614 \pm .08	1.439 \pm .05
		15	75	30	0.424 \pm .00	0.632 \pm .00	0.745 \pm .00	0.245 \pm .01	3.124 \pm .01	8.608 \pm .06	1.372 \pm .05
		15	105	36	0.430 \pm .00	0.635 \pm .00	0.748 \pm .00	0.269 \pm .01	3.114 \pm .01	8.576 \pm .07	1.384 \pm .05

Table B. **Ablation study** on memory configurations for Interact2Ar across different evaluation settings. m_s and m_l represent the context window used for each memory. $m_l = -$ indicates models not using Mixed Memory. For models using Mixed Memory, $\delta = 5$. The total number of frames used in the full memory is $\mathcal{M} = m_s + m_l/\delta$.

sult in more informative generations, it also increases the complexity of the task that the denoiser has to learn, resulting in a non-linear improvement of metrics as the memory size increases. However, what is more noticeable is the significant increase in FID, which is generally used to determine motion quality, when using Mixed Memory.

C. Qualitative Evaluation

In addition to the qualitative examples shown in Fig. 5 and Fig. 6, we introduce a new set of examples and comparisons in the Supplementary Video. Due to the 4D nature of the representation that we generate, images present a significant information loss. In the video, the quality of the motion and the side-by-side comparison will facilitate understanding and highlighting the qualitative differences between Interact2Ar and the previous SOTA, InterMask.

D. Code and Data Availability

All the code and checkpoints related to this paper will be publicly released upon the acceptance of this paper. The code will contain all the codebase used to declare, train, and evaluate Interact2Ar and the new set of evaluators. The checkpoints will include the Interact2Ar checkpoints alongside the checkpoints of the evaluators for providing a more robust and reliable evaluation of future works using Inter-X.